

# Ultrafast Photocurrent Response and High Detectivity in Two-Dimensional MoSe<sub>2</sub>-based Heterojunctions

Christian D. Ornelas, Arthur Bowman, Thayer S. Walmsley, Tianjiao Wang, Kraig Andrews, Zhixian Zhou, and Ya-Qiong Xu\*



Cite This: *ACS Appl. Mater. Interfaces* 2020, 12, 46476–46482



Read Online

ACCESS |

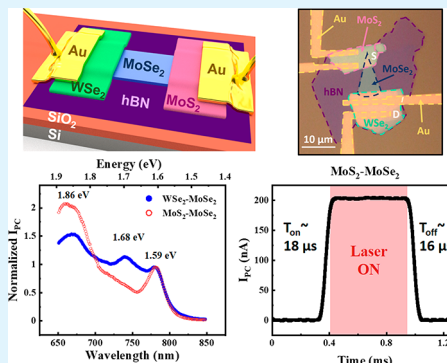
Metrics & More

Article Recommendations

Supporting Information

**ABSTRACT:** Two-dimensional (2D) transition metal dichalcogenide (TMDC) materials have garnered great attention on account of their novel properties and potential to advance modern technology. Recent studies have demonstrated that TMDCs can be utilized to create high-performing heterostructures with combined functionality of the individual layers and new phenomena at these interfaces. Here, we report an ultrafast photoresponse within MoSe<sub>2</sub>-based heterostructures in which heavily p-doped WSe<sub>2</sub> and MoS<sub>2</sub> flakes share an undoped MoSe<sub>2</sub> channel, allowing us to directly compare the optoelectronic properties of MoSe<sub>2</sub>-based heterojunctions with different 2D materials. Strong photocurrent signals have been observed in both MoSe<sub>2</sub>-WSe<sub>2</sub> and MoSe<sub>2</sub>-MoS<sub>2</sub> heterojunctions with a photoresponse time constant of  $\sim 16 \mu\text{s}$ , surmounting previous MoSe<sub>2</sub>-based devices by three orders of magnitude. Further studies have shown that the fast response is independent of the integrated 2D materials (WSe<sub>2</sub> or MoS<sub>2</sub>) but is likely attributed to the high carrier mobility of  $260 \text{ cm}^2 \text{ V}^{-1} \text{ s}^{-1}$  in the undoped MoSe<sub>2</sub> channel as well as the greatly reduced Schottky barriers and near absence of interface states at MoSe<sub>2</sub>-WSe<sub>2</sub>/MoS<sub>2</sub> heterojunctions, which lead to reduced carrier transit time and thus short photocurrent response time. Lastly, a high detectivity on the order of  $\sim 10^{14} \text{ Jones}$  has been achieved in MoSe<sub>2</sub>-based heterojunctions, which supersedes current industry standards. These fundamental studies not only shed light on photocurrent generation mechanisms in MoSe<sub>2</sub>-based heterojunctions but also open up new avenues for engineering future high-performance 2D optoelectronic devices.

**KEYWORDS:** heterojunction, 2D Materials, MoSe<sub>2</sub>, TMDCs, photocurrent



## INTRODUCTION

Two-dimensional (2D) van der Waals (vdW) materials have received considerable attention due to their novel electrical, optical, and mechanical properties as well as the ease of heterostructure fabrication of lattice mismatched materials without strain.<sup>1</sup> In particular, transition metal dichalcogenides (TMDCs) have established themselves as an attractive class of 2D materials as they typically feature sizeable band gaps, strong light–matter interactions, and broad spectral responses.<sup>2</sup> These characteristics naturally facilitate the incorporation of TMDCs into electronic and optoelectronic devices, such as field-effect transistors (FETs),<sup>3–5</sup> photodetectors,<sup>6</sup> photovoltaic cells,<sup>7,8</sup> and many other applications.<sup>9</sup> While some device improvements are achieved through the use of different TMDC channels,<sup>10–12</sup> other works suggest that 2D heterostructures will also enhance device performance.<sup>13–16</sup> Therefore, substantial efforts have been expended in understanding the underlying mechanisms within TMDC heterostructures<sup>17–22</sup> and their commercial synthesis.<sup>23–26</sup> For example, it has been shown that heterostructures consisting of different atomically thin materials like black phosphorus, graphene, and TMDCs can result in devices with improved optoelectronic properties, such as increased mobility and reduced response

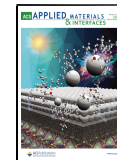
times while foregoing thermal stability in the former examples.<sup>14,27–29</sup> Moreover, heterostructures formed between heavily doped TMDCs and undoped TMDCs display similar enhancements whilst further reducing Schottky barrier heights, resulting in low-resistance ohmic contacts.<sup>30</sup> Such improvements are imperative to attain high-performance optoelectronic devices which allow for the ultrafast movement of information, a highly sought after property of commercial and academic endeavors alike.<sup>31</sup>

Recently, MoSe<sub>2</sub>-based devices have become more prominent as their weakly bound excitons result in intrinsically faster response times.<sup>32</sup> MoSe<sub>2</sub> holds properties indicative of its value in optoelectronic applications, such as a sizable direct band gap of  $\sim 1.6 \text{ eV}$ ,<sup>33,34</sup> high optical absorption,<sup>7</sup> and carrier mobility reaching  $100 \text{ cm}^2 \text{ V}^{-1} \text{ s}^{-1}$ .<sup>35</sup> Despite three-dimensional MoSe<sub>2</sub>-based heterostructures featuring exceedingly fast response

Received: July 5, 2020

Accepted: September 1, 2020

Published: September 1, 2020



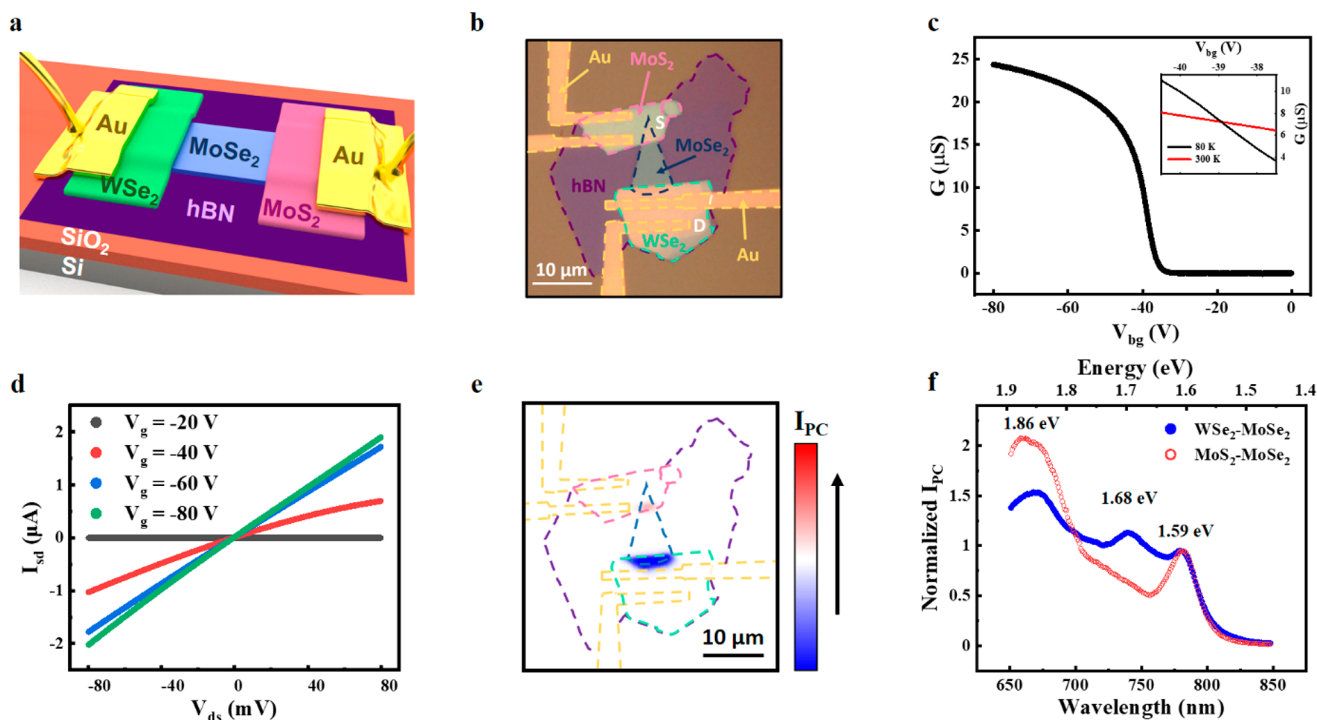


**Figure 1.** (a) Schematic illustrating the composition of a MoSe<sub>2</sub>-based heterostructure. (b) Optical micrograph of a typical device with dashed outlines to indicate the material layout. S and D correspond to source and drain contacts, respectively. (c) Transport characteristics of a device with respect to the back-gate voltage. Inset: the linear region for mobility calculation at 80 K (black) and room temperature (red), respectively. (d)  $I_{ds}$ – $V_{ds}$  characteristics at various back-gate voltages at  $\sim 80$  K. (e) Scanning photocurrent image of the device under  $\sim 30$  mV bias. (f) Normalized wavelength dependence of the photocurrent signals under  $-30$  mV (MoSe<sub>2</sub>–WSe<sub>2</sub>) and  $0$  V (MoSe<sub>2</sub>–MoS<sub>2</sub>) bias voltages, respectively.

times,<sup>36</sup> response times of 2D MoSe<sub>2</sub>-based devices are on the scale of milliseconds,<sup>35,37–39</sup> which are significantly slower than those of commercial semiconductors.<sup>40</sup> Therefore, it is important to investigate MoSe<sub>2</sub>-based heterostructures with inherited unique properties from MoSe<sub>2</sub> plus the fast photoresponse.

In this work, we report the ultrafast photoresponse in MoSe<sub>2</sub>–WSe<sub>2</sub> and MoSe<sub>2</sub>–MoS<sub>2</sub> heterojunctions, where heavily p-doped MoS<sub>2</sub> and WSe<sub>2</sub> flakes are bridged by an undoped MoSe<sub>2</sub> channel. The fast rise and decay time constants (as low as  $\sim 16$   $\mu$ s) have been achieved in both MoSe<sub>2</sub>–WSe<sub>2</sub> and MoSe<sub>2</sub>–MoS<sub>2</sub> heterojunctions. Further studies have shown that the fast photoresponse likely results from the high carrier mobility ( $260$   $\text{cm}^2 \text{V}^{-1}\text{s}^{-1}$ ) as well as negligible Schottky barriers and near absence of interface states at MoSe<sub>2</sub>–WSe<sub>2</sub>/MoS<sub>2</sub> heterojunctions, which are expected to reduce the carrier transit time and thus the photoresponse time. Moreover, a detectivity of  $\sim 10^{14}$  Jones has been observed in MoSe<sub>2</sub>-based heterojunctions, which are higher than commercial Si- and InGaAs-based photodetectors. Our experimental results offer a way to build ultrafast 2D heterojunctions, opening a door for engineering future high-performance 2D optoelectronics.

## EXPERIMENTAL SECTION

**Device Fabrication.** MoSe<sub>2</sub>, heavily p-doped WSe<sub>2</sub> ( $\text{Nb}_{0.005}\text{W}_{0.995}\text{Se}_2$ ), heavily p-doped WSe<sub>2</sub> ( $\text{Nb}_{0.005}\text{M}_{0.995}\text{S}_2$ ), and hBN flakes were mechanically exfoliated from bulk crystals and transferred via a dry transfer method to a silicon substrate with 280 nm of thermally grown SiO<sub>2</sub>. The thickness of each material was identified by noncontact mode atomic force microscopy (Park-System XE-70). Electron beam lithography and subsequent deposition of Au/

Ti were used to form metal electrodes for the heavily p-doped TMDCs.

**Electrical and Optoelectronic Characterization.** All experiments were performed in a Janis ST-500 microscopy cryostat in a high vacuum environment ( $\sim 10^{-6}$  Torr). Current signals were collected via a DL instrument 1211 current preamplifier. Scanning photocurrent measurements were executed using an Olympus BX51WI microscope. A linearly polarized continuous wave laser beam (NKT Photonics SuperK Supercontinuum Laser) was expanded and focused with a 40x objective (N.A. = 0.6) into a diffraction-limited spot ( $\sim 1$   $\mu\text{m}$ ) and scanned over the device by a piezo-controlled mirror with nanometer-scale spatial resolution.

## RESULTS AND DISCUSSION

Figure 1a depicts a schematic diagram of the MoSe<sub>2</sub> heterostructure that consists of an undoped MoSe<sub>2</sub> channel with two asymmetric contacts of heavily p-doped WSe<sub>2</sub> and MoS<sub>2</sub> flakes, respectively, which are connected to Au/Ti electrodes. MoSe<sub>2</sub> has been selected as a channel material, while other TMDCs with distinct band gaps serve as a basis for the choice of contact materials. This not only sheds light on the photocurrent generation mechanisms in TMDC-based heterojunctions but also provides a way to fabricate fast MoSe<sub>2</sub> phototransistors. The device is fabricated on top of a thin flake of hBN to provide a clean substrate and thus to avoid charge traps and surface bonds present on SiO<sub>2</sub>.<sup>41</sup> An optical image of a typical device is presented in Figure 1b, where different materials are outlined with the following color scheme: Au contacts (yellow), hBN (purple), WSe<sub>2</sub> (green), MoSe<sub>2</sub> (blue), and MoS<sub>2</sub> (pink). As shown in Figure S1, the MoS<sub>2</sub> and WSe<sub>2</sub> flakes were  $\sim 23$  nm and  $\sim 16$  nm thick, respectively, while the MoSe<sub>2</sub> channel and hBN were  $\sim 7$  nm and  $\sim 15$  nm, respectively. These materials were mechanically exfoliated

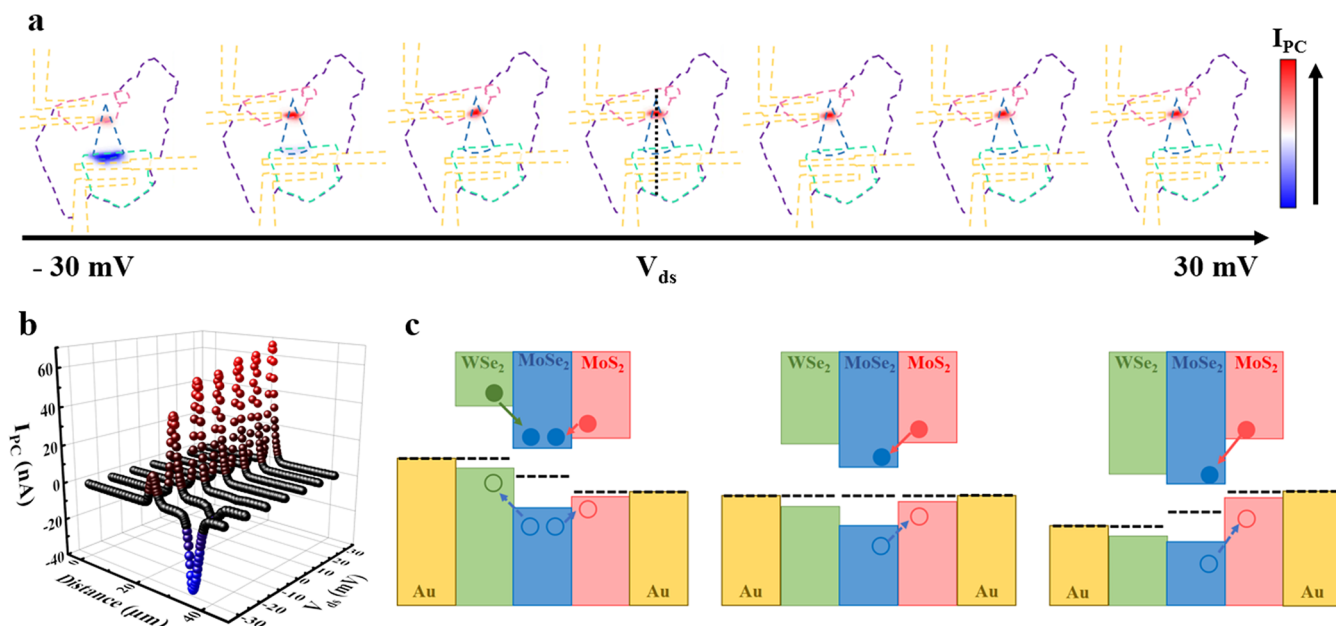


**Figure 2.** (a) Scanning photocurrent signal under various drain-source bias voltages. (b) Numerical representation of photocurrent under different bias voltages along a single scanline, depicted by a dotted line in (a). (c) Band diagrams for the device under  $V_{ds} = -30$  mV, 0V, and 30 mV, respectively.

from bulk crystals, and their thickness was found via atomic force microscopy (AFM). The undoped MoSe<sub>2</sub> and the heavily p-doped TMDC heterojunctions were formed via a dry transfer method. Electron beam lithography and deposition of 50/5 nm Au/Ti were subsequently conducted to form the metal electrodes. A dielectric stack made of 280 nm SiO<sub>2</sub> and a ~15 nm hBN flake facilitates the application of a back-gate voltage to the device. The electrical and optoelectronic properties of this device were investigated under high vacuum ( $\sim 10^{-6}$  Torr) and at a low temperature (80 K) using a Janis ST-500 microscopy cryostat. Figure 1c shows a p-type behavior of the device, which is due to the two heavily p-doped contacts (WSe<sub>2</sub> and MoS<sub>2</sub>) that only allow the MoSe<sub>2</sub> channel to be turned on under a negative gate voltage. The field-effect hole mobilities are extrapolated as  $\sim 260$  cm<sup>2</sup> V<sup>-1</sup> s<sup>-1</sup> at 80 K and  $\sim 70$  cm<sup>2</sup> V<sup>-1</sup> s<sup>-1</sup> at room temperature, respectively, which is higher than previous reports of MoSe<sub>2</sub> devices.<sup>35,42–44</sup> Specifically, the expression used to calculate mobility is  $\mu_{FET} = (1/C_{bg}) \times (L/W) \times (d\sigma/dV_{bg})$ , where  $C_{bg}$  is the back-gate capacitance of the 280 nm thick SiO<sub>2</sub> in series with a ~15 nm hBN flake,  $L$  and  $W$  are the length and average width of the channel, respectively, and the derivative is the extrapolated slope of the linear portion of the transfer curve. Figure 1d displays linear and symmetric output characteristics of the MoSe<sub>2</sub> heterostructure when a wide range of back-gate voltages were applied at 80 K, indicating ohmic behaviors of the device. This suggests that the 2D/2D contacts allow low contact resistance, and the resistances between heavily p-doped TMDCs and external metal electrodes are negligible due to the tunneling effect through an extremely narrow (on the order of nm) depletion region, leading to high hole mobility of our device.<sup>30,34,45</sup>

Next, we explore the optoelectronic properties of the MoSe<sub>2</sub> heterostructure using spatially resolved scanning photocurrent measurements. The positions of the photocurrent signals ( $I_{PC} = I_{laser} - I_{dark}$ ) were precisely located by the correlation of the reflection image of the device with its optical image, as

depicted by Figure 1e, where the red/blue color represents positive/negative photocurrent. As seen in the aforementioned figure, remarkable photocurrent signals are found at both MoSe<sub>2</sub>–WSe<sub>2</sub> and MoSe<sub>2</sub>–MoS<sub>2</sub> heterojunctions. To further investigate the contrasting characteristics of these heterojunctions, the wavelength-dependent photocurrent measurements were conducted with a focused beam. Here, the device was explored under the drain-source bias of -30 mV and zero bias for MoSe<sub>2</sub>–WSe<sub>2</sub> and MoSe<sub>2</sub>–MoS<sub>2</sub> heterojunctions, respectively. Figure 1f shows a photocurrent peak at  $\sim 1.59$  eV detected in both heterojunctions, which is likely related to the A exciton energy of few-layer MoSe<sub>2</sub>.<sup>46</sup> This observation indicates that the photocurrent signals mainly result from the optical absorption of the MoSe<sub>2</sub> channel under 780 nm illumination. Moreover, a photocurrent peak is observed at  $\sim 1.68$  eV in the MoSe<sub>2</sub>–WSe<sub>2</sub> heterojunction, which is close to the A exciton energy of WSe<sub>2</sub>.<sup>22,47</sup> This suggests that the p-doped WSe<sub>2</sub> flake also contributes to the photocurrent generation at the heterojunctions. Interestingly, a maximum photocurrent signal is found at both heterojunctions for wavelengths with energies surrounding  $\sim 1.84$  eV, which may be attributed to the B exciton energy of the MoSe<sub>2</sub> channel.<sup>48,49</sup> We also know that the A exciton energy of few-layer MoS<sub>2</sub> occurs in this region of the spectrum (1.8 – 1.9 eV).<sup>50,51</sup> Indeed, the photocurrent intensity of the MoSe<sub>2</sub>–MoS<sub>2</sub> heterojunction is higher than that of the MoSe<sub>2</sub>–WSe<sub>2</sub> heterojunction under 674 nm illumination, suggesting that the contribution from the optical absorption of the p-doped MoS<sub>2</sub> flake cannot be neglected. Our experimental results indicate that both the undoped MoSe<sub>2</sub> and p-doped MoS<sub>2</sub>/WSe<sub>2</sub> flakes contribute to the photocurrent generations in these heterojunctions.

To further elucidate the photoresponse generation mechanisms of MoSe<sub>2</sub>-based heterojunctions, bias-dependent scanning photocurrent measurements were performed by sweeping the drain-source bias voltages from -30 to 30 mV. The resulting photocurrent mappings of the device are depicted in

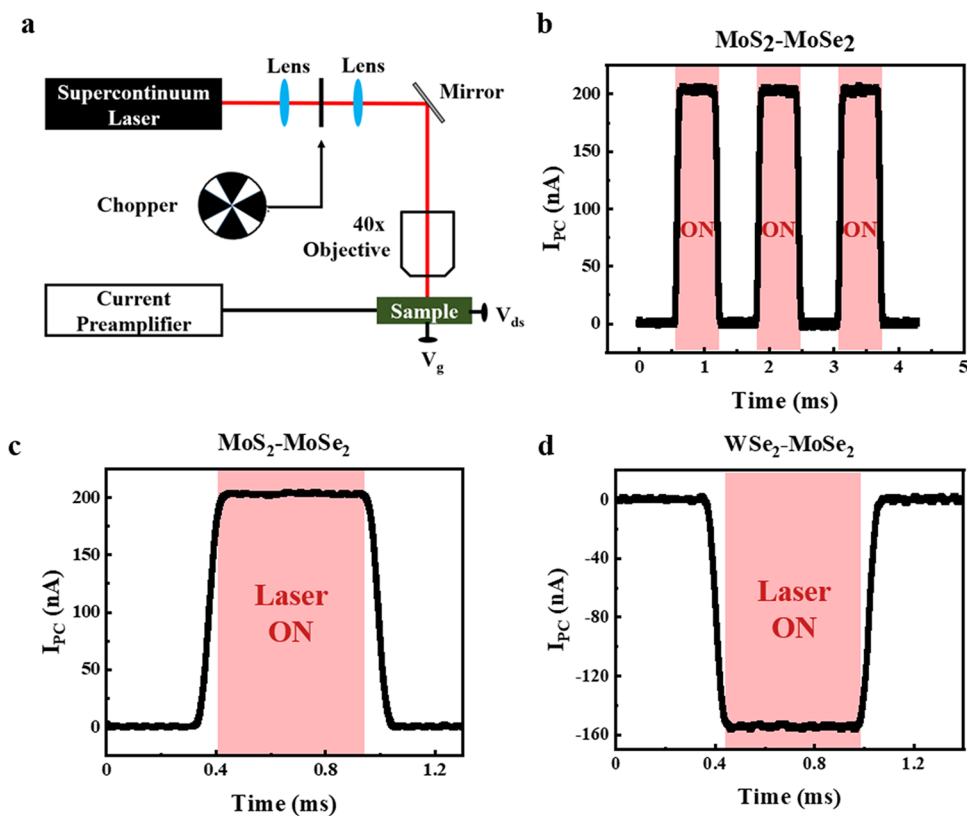


**Figure 3.** (a) Diagram depicting the experimental setup used to measure time-dependent photocurrent signals. (b) Photocurrent responses as a function of time under 650 nm illumination. The photocurrent signals were collected for the (c)  $\text{MoSe}_2$ – $\text{MoS}_2$  junction under zero bias and the (d)  $\text{MoSe}_2$ – $\text{WSe}_2$  junction with  $V_{\text{ds}} = -30$  mV, respectively.

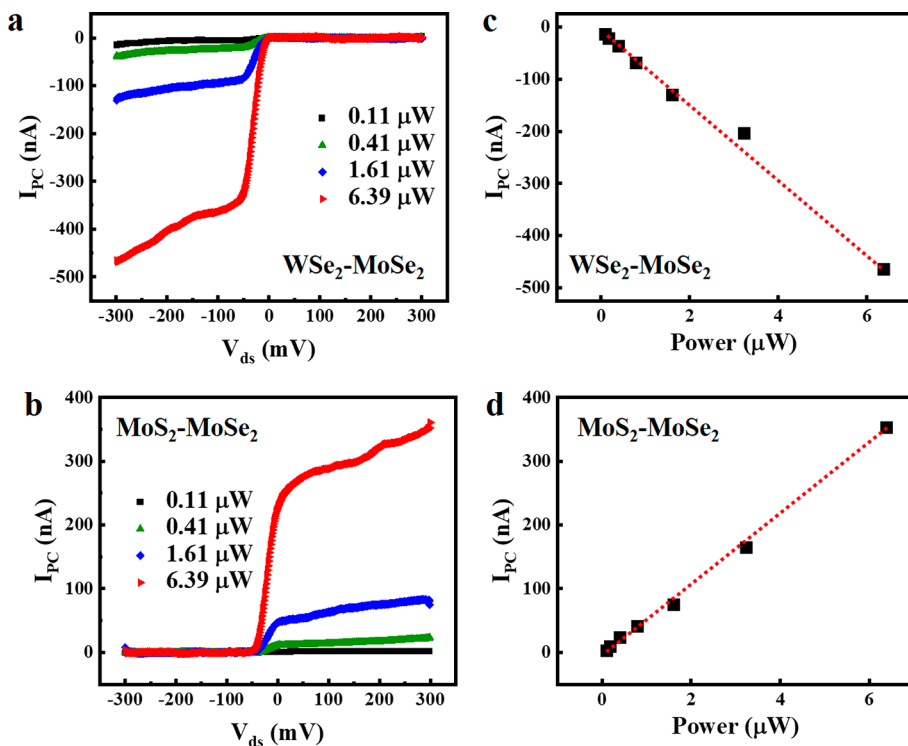


**Figure 4.** Photocurrent signals as a function of drain-source bias under a zero gate voltage ( $\lambda = 650$  nm) on (a)  $\text{MoSe}_2$ – $\text{WSe}_2$  and (b)  $\text{MoSe}_2$ – $\text{MoS}_2$  junctions, respectively. Power dependence of photocurrent responses on (c)  $\text{MoSe}_2$ – $\text{WSe}_2$  and (d)  $\text{MoSe}_2$ – $\text{MoS}_2$  junctions, respectively.

Figure 2a, while quantitative measurements of photocurrent are extracted along the black dotted line and plotted spatially in Figure 2b. Under zero bias, photocurrent responses are primarily observed at the MoSe<sub>2</sub>–MoS<sub>2</sub> junction, where electron-hole pairs (EHPs) are separated by a band offset between the heavily p-doped MoS<sub>2</sub> and undoped MoSe<sub>2</sub> flakes, leading to a current from MoSe<sub>2</sub> to MoS<sub>2</sub>. The relatively weak photocurrent response at the MoSe<sub>2</sub>–WSe<sub>2</sub> junction is likely attributed to a smaller band offset between the MoSe<sub>2</sub> and WSe<sub>2</sub>, suggesting that the p-doping level in the WSe<sub>2</sub> flake is slightly lower than that in the MoS<sub>2</sub> flake. When the bias is increased to 30 mV, the band offset at the MoSe<sub>2</sub>–MoS<sub>2</sub> junction increases, and consequently, the photocurrent intensity is enhanced. On the other hand, when the device is under a negative bias voltage of −30 mV, negative photocurrent signals begin to appear at the MoSe<sub>2</sub>–WSe<sub>2</sub> heterojunction, which may result from the increase in the band offset between the undoped MoSe<sub>2</sub> and p-doped WSe<sub>2</sub> flakes. Here, the photoexcited holes can flow from MoSe<sub>2</sub> to WSe<sub>2</sub> and thus generate negative photocurrent responses at this heterojunction. These behaviors are depicted in Figure 2c and Figure S2.

The temporal response of the device was subsequently explored using an ON/OFF light modulation accomplished by the addition of an optical chopper to the laser path, as shown in Figure 3a. The photocurrent signals can be plotted versus time (Figure 3b), where the rise and decay time constants of the signals are extracted with a single exponential fitting function. Under zero bias, where the MoSe<sub>2</sub>–MoS<sub>2</sub> heterojunction features sizable photocurrent signals, the rise and decay time constants are ~18 μs and ~16 μs (Figure 3c), respectively, which are three orders of magnitude faster than previous 2D MoSe<sub>2</sub>-based phototransistors<sup>4,10,38,39,52–57</sup> and is comparable with other 2D TMDC phototransistors.<sup>29,58</sup> Interestingly, the rise and decay time constants for the MoSe<sub>2</sub>–WSe<sub>2</sub> heterojunction under −30 mV bias are ~17 μs (Figure 3d), which are similar to those of the MoSe<sub>2</sub>–MoS<sub>2</sub> heterojunction. The ultrafast photoresponse in MoSe<sub>2</sub>-based heterojunctions is likely attributed to their unique 2D/2D heterostructures, where the near absence of interface states at the MoSe<sub>2</sub>–WSe<sub>2</sub> and MoSe<sub>2</sub>–MoS<sub>2</sub> van der Waals heterojunctions can significantly reduce charge trapping compared to conventional metal–2D semiconductor junctions, where interface states are almost ubiquitous. (More details are present in the Supporting Information.) In addition, the high mobility of 260 cm<sup>2</sup> V<sup>−1</sup> s<sup>−1</sup> in the MoSe<sub>2</sub> channel on the hBN substrate and the greatly lowered Schottky barriers at the heterojunction contacts are expected to reduce transit time and thus shorten photoresponse time. Furthermore, the photoexcited carriers can be easily collected by the external metal electrodes through the tunneling effect due to the narrow depletion region between heavily doped TMDCs and metal electrodes.

The performance of the MoSe<sub>2</sub> heterostructure device was subsequently assessed when the device is in the OFF state with a negligible dark current of ~10<sup>−10</sup> A. Figure 4a,b shows the photocurrent signals of the MoSe<sub>2</sub>-based heterojunctions with various laser powers when the drain-source bias voltages are swept from −300 to 300 mV. The photocurrent signals of the MoSe<sub>2</sub>–WSe<sub>2</sub> junction are negligible for zero and positive bias voltages, while exponentially increasing as the bias changes from zero to approximately −50 mV. As the negative bias further increases beyond −50 mV, the photocurrent signals at

the MoSe<sub>2</sub>–WSe<sub>2</sub> junction increase at a much slower rate. On the other hand, the MoSe<sub>2</sub>–MoS<sub>2</sub> junction features substantial photocurrent signals even under zero bias, which slowly increase with an increasing positive bias voltage. As the bias changes from zero to negative, the photocurrent signals drop rapidly and nearly diminish at −50 mV. The photocurrent intensity shows a linear dependence on laser power with maximum photoresponsivities of ~140<sup>−1</sup> and ~60 mA W<sup>−1</sup> for MoSe<sub>2</sub>–WSe<sub>2</sub> and MoSe<sub>2</sub>–MoS<sub>2</sub> junctions (Figure 4c,d), respectively, suggesting that photocurrent generation is directly proportional to absorption of incident photons.<sup>59</sup> Furthermore, the MoSe<sub>2</sub>-based heterojunctions demonstrate a high specific detectivity on the order of ~10<sup>14</sup> Jones, a value better than state-of-the-art devices frequently used for photodetection.<sup>60</sup>

## CONCLUSIONS

In conclusion, we report MoSe<sub>2</sub>-based heterostructures with a fast photoresponse of as low as ~16 μs, which is three orders of magnitudes faster than previously reported values for MoSe<sub>2</sub>-based devices. Moreover, detectivity on the order of ~10<sup>14</sup> Jones has been achieved in our MoSe<sub>2</sub>-based heterojunctions, greater than current industry standards. Further studies have shown that the ultrafast photoresponse is not dependent on the integrated TMDC materials (either heavily p-doped WSe<sub>2</sub> or MoS<sub>2</sub>) in MoSe<sub>2</sub>-based heterojunctions, but it is likely attributed to the high hole mobility (260 cm<sup>2</sup> V<sup>−1</sup> s<sup>−1</sup>) and negligible contact resistance at 2D/2D interfaces,<sup>30</sup> which are expected to foster carrier transit time and thus shorten the photocurrent response times. These results suggest that ultrafast performance can be attained within MoSe<sub>2</sub>-based heterojunctions, providing a way to build future ultrafast 2D optoelectronics.

## ASSOCIATED CONTENT

### Supporting Information

The Supporting Information is available free of charge at <https://pubs.acs.org/doi/10.1021/acsami.0c12155>.

Thickness of different materials, energy levels of different materials, and mechanisms for a fast photocurrent response (PDF)

## AUTHOR INFORMATION

### Corresponding Author

Ya-Qiong Xu – Department of Physics and Astronomy and Department of Electrical Engineering and Computer Science, Vanderbilt University, Nashville, Tennessee 37235, United States of America; [orcid.org/0000-0003-1423-7458](https://orcid.org/0000-0003-1423-7458); Email: [yaqiong.xu@vanderbilt.edu](mailto:yaqiong.xu@vanderbilt.edu)

### Authors

Christian D. Ornelas – Department of Physics and Astronomy, Vanderbilt University, Nashville, Tennessee 37235, United States of America

Arthur Bowman – Department of Physics and Astronomy, Wayne State University, Detroit, Michigan 48201, United States of America

Thayer S. Walmsley – Department of Physics and Astronomy, Vanderbilt University, Nashville, Tennessee 37235, United States of America

Tianjiao Wang – Department of Electrical Engineering and Computer Science, Vanderbilt University, Nashville, Tennessee 37235, United States

**Kraig Andrews** — Department of Physics and Astronomy, Wayne State University, Detroit, Michigan 48201, United States of America

**Zhixian Zhou** — Department of Physics and Astronomy, Wayne State University, Detroit, Michigan 48201, United States of America;  [orcid.org/0000-0002-9228-4260](https://orcid.org/0000-0002-9228-4260)

Complete contact information is available at:  
<https://pubs.acs.org/10.1021/acsami.0c12155>

## Notes

The authors declare no competing financial interest.

## ACKNOWLEDGMENTS

This work was supported by the National Science Foundation (ECCS-1810088, CBET-1805924, and DMR-2004445).

## REFERENCES

- (1) Zhang, H. Ultrathin Two-Dimensional Nanomaterials. *ACS Nano* **2015**, *9*, 9451–9469.
- (2) Choi, W.; Choudhary, N.; Han, G. H.; Park, J.; Akinwande, D.; Lee, Y. H. Recent Development of Two-Dimensional Transition Metal Dichalcogenides and Their Applications. *Mater. Today* **2017**, *116*–130.
- (3) Pudasaini, P. R.; Stanford, M. G.; Oyedele, A.; Wong, A. T.; Hoffman, A. N.; Briggs, D. P.; Xiao, K.; Mandrus, D. G.; Ward, T. Z.; Rack, P. D. High Performance Top-Gated Multilayer WSe<sub>2</sub> Field Effect Transistors. *Nanotechnology* **2017**, *28*, 475202.
- (4) Radisavljevic, B.; Radenovic, A.; Brivio, J.; Giacometti, V.; Kis, A. Single-Layer MoS<sub>2</sub> Transistors. *Nat. Nanotechnol.* **2011**, *6*, 147–150.
- (5) Lin, J.; Zhong, J.; Zhong, S.; Li, H.; Zhang, H.; Chen, W. Modulating Electronic Transport Properties of MoS<sub>2</sub> Field Effect Transistor by Surface Overlays. *Appl. Phys. Lett.* **2013**, *103*, No. 063109.
- (6) Xue, Y.; Zhang, Y.; Liu, Y.; Liu, H.; Song, J.; Sophia, J.; Liu, J.; Xu, Z.; Xu, Q.; Wang, Z.; Zheng, J.; Liu, Y.; Li, S.; Bao, Q. Scalable Production of a Few-Layer MoS<sub>2</sub>/WS<sub>2</sub> Vertical Heterojunction Array and Its Application for Photodetectors. *ACS Nano* **2016**, *10*, 573–580.
- (7) Bernardi, M.; Palummo, M.; Grossman, J. C. Extraordinary Sunlight Absorption and One Nanometer Thick Photovoltaics Using Two-Dimensional Monolayer Materials. *Nano Lett.* **2013**, *13*, 3664–3670.
- (8) Flöry, N.; Jain, A.; Bharadwaj, P.; Parzefall, M.; Taniguchi, T.; Watanabe, K.; Novotny, L. A WSe<sub>2</sub>/MoSe<sub>2</sub> Heterostructure Photovoltaic Device. *Appl. Phys. Lett.* **2015**, *107*, 123106.
- (9) Bhimanapati, G. R.; Lin, Z.; Meunier, V.; Jung, Y.; Cha, J.; Das, S.; Xiao, D.; Son, Y.; Strano, M. S.; Cooper, V. R.; Liang, L.; Louie, S. G.; Ringe, E.; Zhou, W.; Kim, S. S.; Naik, R. R.; Sumpter, B. G.; Terrones, H.; Xia, F.; Wang, Y.; Zhu, J.; Akinwande, D.; Alem, N.; Schuller, J. A.; Schaak, R. E.; Terrones, M.; Robinson, J. A. Recent Advances in Two-Dimensional Materials beyond Graphene. *ACS Nano* **2015**, *9*, 11509–11539.
- (10) Lopez-Sanchez, O.; Lembke, D.; Kayci, M.; Radenovic, A.; Kis, A. Ultrasensitive Photodetectors Based on Monolayer MoS<sub>2</sub>. *Nat. Nanotechnol.* **2013**, *8*, 497–501.
- (11) Choi, W.; Cho, M. Y.; Konar, A.; Lee, J. H.; Cha, G. B.; Hong, S. C.; Kim, S.; Kim, J.; Jena, D.; Joo, J.; Kim, S. High-Detectivity Multilayer MoS<sub>2</sub> Phototransistors with Spectral Response from Ultraviolet to Infrared. *Adv. Mater.* **2012**, *24*, 5832–5836.
- (12) Xie, C.; Mak, C.; Tao, X.; Yan, F. Photodetectors Based on Two-Dimensional Layered Materials Beyond Graphene. *Adv. Funct. Mater.* **2017**, *27*, 1603886.
- (13) Huo, N.; Kang, J.; Wei, Z.; Li, S.-S.; Li, J.; Wei, S.-H. Novel and Enhanced Optoelectronic Performances of Multilayer MoS<sub>2</sub>-WS<sub>2</sub> Heterostructure Transistors. *Adv. Funct. Mater.* **2014**, *24*, 7025–7031.
- (14) Ye, L.; Li, H.; Chen, Z.; Xu, J. Near-Infrared Photodetector Based on MoS<sub>2</sub>/Black Phosphorus Heterojunction. *ACS Photonics* **2016**, *3*, 692–699.
- (15) Georgiou, T.; Jalil, R.; Belle, B. D.; Britnell, L.; Gorbachev, R. V.; Morozov, S. V.; Kim, Y.-J.; Gholinia, A.; Haigh, S. J.; Makarovskiy, O.; Eaves, L.; Ponomarenko, L. A.; Geim, A. K.; Novoselov, K. S.; Mishchenko, A. Vertical Field-Effect Transistor Based on Graphene–WS<sub>2</sub> Heterostructures for Flexible and Transparent Electronics. *Nat. Nanotechnol.* **2013**, *8*, 100–103.
- (16) Yu, W. J.; Liu, Y.; Zhou, H.; Yin, A.; Li, Z.; Huang, Y.; Duan, X. Highly Efficient Gate-Tunable Photocurrent Generation in Vertical Heterostructures of Layered Materials. *Nat. Nanotechnol.* **2013**, *8*, 952–958.
- (17) Ross, J. S.; Rivera, P.; Schaibley, J.; Lee-Wong, E.; Yu, H.; Taniguchi, T.; Watanabe, K.; Yan, J.; Mandrus, D.; Cobden, D.; Yao, W.; Xu, X. Interlayer Exciton Optoelectronics in a 2D Heterostructure p–n Junction. *Nano Lett.* **2017**, *17*, 638–643.
- (18) Zhang, N.; Surrente, A.; Baranowski, M.; Maude, D. K.; Gant, P.; Castellanos-Gomez, A.; Plochocka, P. Moiré Intralayer Excitons in a MoSe<sub>2</sub>/MoS<sub>2</sub> Heterostructure. *Nano Lett.* **2018**, *18*, 7651–7657.
- (19) Ben Amara, I.; Ben Salem, E.; Jaziri, S. Optoelectronic Response and Interlayer Exciton Features of MoS<sub>2</sub>/WS<sub>2</sub> Van Der Waals Heterostructure within First Principle Calculations and Wannier Mott Model. *Superlattices Microstruct.* **2017**, *109*, 897–904.
- (20) Baranowski, M.; Surrente, A.; Kłopotowski, L.; Urban, J. M.; Zhang, N.; Maude, D. K.; Wiwatowski, K.; Mackowski, S.; Kung, Y. C.; Dumcenco, D.; Kis, A.; Plochocka, P. Probing the Interlayer Exciton Physics in a MoS<sub>2</sub> /MoSe<sub>2</sub> /MoS<sub>2</sub> van Der Waals Heterostructure. *Nano Lett.* **2017**, *17*, 6360–6365.
- (21) Rivera, P.; Seyler, K. L.; Yu, H.; Schaibley, J. R.; Yan, J.; Mandrus, D. G.; Yao, W.; Xu, X. Valley-Polarized Exciton Dynamics in a 2D Semiconductor Heterostructure. *Science* **2016**, *351*, 688–691.
- (22) Hanbicki, A. T.; Chuang, H.-J.; Rosenberger, M. R.; Hellberg, C. S.; Sivaram, S. V.; McCreary, K. M.; Mazin, I. I.; Jonker, B. T. Double Indirect Interlayer Exciton in a MoSe<sub>2</sub>/WSe<sub>2</sub> van Der Waals Heterostructure. *ACS Nano* **2018**, *12*, 4719–4726.
- (23) Gong, Y.; Lei, S.; Ye, G.; Li, B.; He, Y.; Keyshar, K.; Zhang, X.; Wang, Q.; Lou, J.; Liu, Z.; Vajtai, R.; Zhou, W.; Ajayan, P. M. Two-Step Growth of Two-Dimensional WSe<sub>2</sub> /MoSe<sub>2</sub> Heterostructures. *Nano Lett.* **2015**, *15*, 6135–6141.
- (24) Solís-Fernández, P.; Bissett, M.; Ago, H. Synthesis, Structure and Applications of Graphene-Based 2D Heterostructures. *Chem. Soc. Rev.* **2017**, *46*, 4572–4613.
- (25) Tongay, S.; Fan, W.; Kang, J.; Park, J.; Koldemir, U.; Suh, J.; Narang, D. S.; Liu, K.; Ji, J.; Li, J.; Sinclair, R.; Wu, J. Tuning Interlayer Coupling in Large-Area Heterostructures with CVD-Grown MoS<sub>2</sub> and WS<sub>2</sub> Monolayers. *Nano Lett.* **2014**, *14*, 3185–3190.
- (26) Duan, X.; Wang, C.; Shaw, J. C.; Cheng, R.; Chen, Y.; Li, H.; Wu, X.; Tang, Y.; Zhang, Q.; Pan, A.; Jiang, J.; Yu, R.; Huang, Y.; Duan, X. Lateral Epitaxial Growth of Two-Dimensional Layered Semiconductor Heterojunctions. *Nat. Nanotechnol.* **2014**, *9*, 1024–1030.
- (27) Das, S.; Gulotty, R.; Sumant, A. V.; Roelofs, A. All Two-Dimensional, Flexible, Transparent, and Thinnest Thin Film Transistor. *Nano Lett.* **2014**, *14*, 2861–2866.
- (28) Deng, Y.; Luo, Z.; Conrad, N. J.; Liu, H.; Gong, Y.; Najmaei, S.; Ajayan, P. M.; Lou, J.; Xu, X.; Ye, P. D. Black Phosphorus–Monolayer MoS<sub>2</sub> van Der Waals Heterojunction p–n Diode. *ACS Nano* **2014**, *8*, 8292–8299.
- (29) Walmsley, T. S.; Chamlagain, B.; Rijal, U.; Wang, T.; Zhou, Z.; Xu, Y. Gate-Tunable Photoresponse Time in Black Phosphorus–MoS<sub>2</sub> Heterojunctions. *Adv. Opt. Mater.* **2019**, *7*, 1800832.
- (30) Chuang, H.-J.; Chamlagain, B.; Koehler, M.; Perera, M. M.; Yan, J.; Mandrus, D.; Tománek, D.; Zhou, Z. Low-Resistance 2D/2D Ohmic Contacts: A Universal Approach to High-Performance WSe<sub>2</sub>, MoS<sub>2</sub>, and MoSe<sub>2</sub> Transistors. *Nano Lett.* **2016**, *16*, 1896–1902.
- (31) Long, M.; Wang, P.; Fang, H.; Hu, W. Progress, Challenges, and Opportunities for 2D Material Based Photodetectors. *Adv. Funct. Mater.* **2019**, *1*–28.

(32) Chang, Y.-H.; Zhang, W.; Zhu, Y.; Han, Y.; Pu, J.; Chang, J.-K.; Hsu, W.-T.; Huang, J.-K.; Hsu, C.-L.; Chiu, M.-H.; Takenobu, T.; Li, H.; Wu, C.-I.; Chang, W.-H.; Wee, A. T. S.; Li, L.-J. Monolayer MoSe<sub>2</sub> Grown by Chemical Vapor Deposition for Fast Photodetection. *ACS Nano* **2014**, *8*, 8582–8590.

(33) Tongay, S.; Zhou, J.; Ataca, C.; Lo, K.; Matthews, T. S.; Li, J.; Grossman, J. C.; Wu, J. Thermally Driven Crossover from Indirect toward Direct Bandgap in 2D Semiconductors: MoSe<sub>2</sub> versus MoS<sub>2</sub>. *Nano Lett.* **2012**, *12*, 5576–5580.

(34) Zhang, Y.; Chang, T.-R.; Zhou, B.; Cui, Y.-T.; Yan, H.; Liu, Z.; Schmitt, F.; Lee, J.; Moore, R.; Chen, Y.; Lin, H.; Jeng, H.-T.; Mo, S.-K.; Hussain, Z.; Bansil, A.; Shen, Z.-X. Direct Observation of the Transition from Indirect to Direct Bandgap in Atomically Thin Epitaxial MoSe<sub>2</sub>. *Nat. Nanotechnol.* **2014**, *9*, 111–115.

(35) Lee, H.; Ahn, J.; Im, S.; Kim, J.; Choi, W. High-Responsivity Multilayer MoSe<sub>2</sub> Phototransistors with Fast Response Time. *Sci. Rep.* **2018**, *8*, 11545.

(36) Mao, J.; Yu, Y.; Wang, L.; Zhang, X.; Wang, Y.; Shao, Z.; Jie, J. Ultrafast, Broadband Photodetector Based on MoSe<sub>2</sub> /Silicon Heterojunction with Vertically Standing Layered Structure Using Graphene as Transparent Electrode. *Adv. Sci.* **2016**, *3*, 1600018.

(37) Abderrahmane, A.; Ko, P. J.; Thu, T. V.; Ishizawa, S.; Takamura, T.; Sandhu, A. High Photosensitivity Few-Layered MoSe<sub>2</sub> Back-Gated Field-Effect Phototransistors. *Nanotechnology* **2014**, *25*, 365202.

(38) Jung, C.; Kim, S. M.; Moon, H.; Han, G.; Kwon, J.; Hong, Y. K.; Omkaram, I.; Yoon, Y.; Kim, S.; Park, J. Highly Crystalline CVD-Grown Multilayer MoSe<sub>2</sub> Thin Film Transistor for Fast Photodetector. *Sci. Rep.* **2015**, *5*, 15313.

(39) Rivera, P.; Schaibley, J. R.; Jones, A. M.; Ross, J. S.; Wu, S.; Aivazian, G.; Klement, P.; Seyler, K.; Clark, G.; Ghimire, N. J.; Yan, J.; Mandrus, D. G.; Yao, W.; Xu, X. Observation of Long-Lived Interlayer Excitons in Monolayer MoSe<sub>2</sub>–WSe<sub>2</sub> Heterostructures. *Nat. Commun.* **2015**, *6*, 6242.

(40) Hamamatsu. Si Photodiodes E. 2014, No. February, 1–6.

(41) Dean, C. R.; Young, A. F.; Meric, I.; Lee, C.; Wang, L.; Sorgenfrei, S.; Watanabe, K.; Taniguchi, T.; Kim, P.; Shepard, K. L.; Hone, J. Boron Nitride Substrates for High-Quality Graphene Electronics. *Nat. Nanotechnol.* **2010**, *5*, 722–726.

(42) Larentis, S.; Fallahazad, B.; Tutuc, E. Field-Effect Transistors and Intrinsic Mobility in Ultra-Thin MoSe<sub>2</sub> Layers. *Appl. Phys. Lett.* **2012**, *101*, 223104.

(43) Chamlagain, B.; Li, Q.; Ghimire, N. J.; Chuang, H.-J.; Perera, M. M.; Tu, H.; Xu, Y.; Pan, M.; Xaio, D.; Yan, J.; Mandrus, D.; Zhou, Z. Mobility Improvement and Temperature Dependence in MoSe<sub>2</sub> Field-Effect Transistors on Parylene-C Substrate. *ACS Nano* **2014**, *8*, 5079–5088.

(44) Rhyee, J.-S.; Kwon, J.; Dak, P.; Kim, J. H.; Kim, S. M.; Park, J.; Hong, Y. K.; Song, W. G.; Omkaram, I.; Alam, M. A.; Kim, S. High-Mobility Transistors Based on Large-Area and Highly Crystalline CVD-Grown MoSe<sub>2</sub> Films on Insulating Substrates. *Adv. Mater.* **2016**, *28*, 2316–2321.

(45) Wang, T.; Andrews, K.; Bowman, A.; Hong, T.; Koehler, M.; Yan, J.; Mandrus, D.; Zhou, Z.; Xu, Y.-Q. High-Performance WSe<sub>2</sub> Phototransistors with 2D/2D Ohmic Contacts. *Nano Lett.* **2018**, *18*, 2766–2771.

(46) Quereda, J.; Ghiasi, T. S.; van Zwol, F. A.; van der Wal, C. H.; van Wees, B. J. Observation of Bright and Dark Exciton Transitions in Monolayer MoSe<sub>2</sub> by Photocurrent Spectroscopy. *2D Mater.* **2017**, *5*, No. 015004.

(47) He, K.; Kumar, N.; Zhao, L.; Wang, Z.; Mak, K. F.; Zhao, H.; Shan, J. Tightly Bound Excitons in Monolayer WSe<sub>2</sub>. *Phys. Rev. Lett.* **2014**, *113*, No. 026803.

(48) Wang, G.; Gerber, I. C.; Bouet, L.; Lagarde, D.; Balocchi, A.; Vidal, M.; Amand, T.; Marie, X.; Urbaszek, B. Exciton States in Monolayer MoSe<sub>2</sub> : Impact on Interband Transitions. *2D Mater.* **2015**, *2*, No. 045005.

(49) Arora, A.; Nogajewski, K.; Molas, M.; Koperski, M.; Potemski, M. Exciton Band Structure in Layered MoSe<sub>2</sub> : From a Monolayer to the Bulk Limit. *Nanoscale* **2015**, *7*, 20769–20775.

(50) Kumar, A.; Ahluwalia, P. K. Electronic Structure of Transition Metal Dichalcogenides Monolayers 1H-MX<sub>2</sub> (M = Mo, W; X = S, Se, Te) from Ab-Initio Theory: New Direct Band Gap Semiconductors. *Eur. Phys. J. B* **2012**, *85*, 186.

(51) Mak, K. F.; Lee, C.; Hone, J.; Shan, J.; Heinz, T. F. Atomically Thin MoS<sub>2</sub>: A New Direct-Gap Semiconductor. *Phys. Rev. Lett.* **2010**, *105*, 136805.

(52) Wang, B.; Yang, S.; Wang, C.; Wu, M.; Huang, L.; Liu, Q.; Jiang, C. Enhanced Current Rectification and Self-Powered Photoresponse in Multilayer p-MoTe<sub>2</sub>/n-MoS<sub>2</sub> van Der Waals Heterojunctions. *Nanoscale* **2017**, *9*, 10733–10740.

(53) Perea-López, N.; Elías, A. L.; Berkdemir, A.; Castro-Beltran, A.; Gutiérrez, H. R.; Feng, S.; Lv, R.; Hayashi, T.; López-Urías, F.; Ghosh, S.; Muchharla, B.; Talapatra, S.; Terrones, H.; Terrones, M. Photosensor Device Based on Few-Layered WS<sub>2</sub> Films. *Adv. Funct. Mater.* **2013**, *23*, 5511–5517.

(54) Groenendijk, D. J.; Buscema, M.; Steele, G. A.; Michaelis de Vasconcellos, S.; Bratschitsch, R.; van der Zant, H. S. J.; Castellanos-Gomez, A. Photovoltaic and Photothermoelectric Effect in a Double-Gated WSe<sub>2</sub> Device. *Nano Lett.* **2014**, *14*, 5846–5852.

(55) Tang, W.; Liu, C.; Wang, L.; Chen, X.; Luo, M.; Guo, W.; Wang, S.-W.; Lu, W. MoS<sub>2</sub> Nanosheet Photodetectors with Ultrafast Response. *Appl. Phys. Lett.* **2017**, *111*, 153502.

(56) Qin, J.-K.; Ren, D.-D.; Shao, W.-Z.; Li, Y.; Miao, P.; Sun, Z.-Y.; Hu, P.; Zhen, L.; Xu, C.-Y. Photoresponse Enhancement in Monolayer ReS<sub>2</sub> Phototransistor Decorated with CdSe–CdS–ZnS Quantum Dots. *ACS Appl. Mater. Interfaces* **2017**, *9*, 39456–39463.

(57) Moun, M.; Singh, A.; Tak, B. R.; Singh, R. Study of the Photoresponse Behavior of a High Barrier Pd/MoS<sub>2</sub>/Pd Photodetector. *J. Phys. D: Appl. Phys.* **2019**, *52*, 325102.

(58) Pradhan, N. R.; Ludwig, J.; Lu, Z.; Rhodes, D.; Bishop, M. M.; Thirunavukkaran, K.; McGill, S. A.; Smirnov, D.; Balicas, L. High Photoresponsivity and Short Photoresponse Times in Few-Layered WSe<sub>2</sub> Transistors. *ACS Appl. Mater. Interfaces* **2015**, *7*, 12080–12088.

(59) Zhang, W.; Huang, J.-K.; Chen, C.-H.; Chang, Y.-H.; Cheng, Y.-J.; Li, L.-J. High-Gain Phototransistors Based on a CVD MoS<sub>2</sub> Monolayer. *Adv. Mater.* **2013**, *25*, 3456–3461.

(60) Wojtas, J.; Mikolajczyk, J.; Bielecki, Z. Aspects of the Application of Cavity Enhanced Spectroscopy to Nitrogen Oxides Detection. *Sensors* **2013**, *13*, 7570–7598.